Optical fibres embedded with as-grown carbon nanotubes for ultrahigh nonlinear optical responses

Qi Xiao, Jin Xie, Guangjie Yao, Kaifeng Lin, Hao-Li Zhang*, Liu Qian*, Kaihui Liu* and Jin Zhang*

Q. Xiao, Prof. J. Zhang*

Beijing Science and Engineering Center for Nanocarbons, School of Materials Science and Engineering, College of Chemistry and Molecular Engineering

Peking University, Beijing 100871, P. R. China.

E-mail: jinzhang@pku.edu.cn

Jin Xie, Guang-jie Yao, Kaifeng Lin, Prof. K.H. Liu*

State Key Laboratory for Mesoscopic Physics, Academy for Advanced Interdisciplinary Studies, School of Physics,

Peking University, Beijing 100871, P. R. China.

E-mail: khliu@pku.edu.cn

This article has been accepted for publication and undergone full peer review but has not been through the copyediting, typesetting, pagination and proofreading process, which may lead to differences between this version and the Version of Record. Please cite this article as doi: 10.1002/adma.202303046.

Dr. L. Qian*

School of Materials Science and Engineering,

Peking University, Beijing, 100871, China.

Q. Xiao, Prof. Hao-Li Zhang*

State Key Laboratory of Applied Organic Chemistry, Key Laboratory of Special Function Materials and Structure Design, College of Chemistry and Chemical Engineering

Lanzhou University, Lanzhou 730000, P. R. China

These authors contributed equally: Qi Xiao, Jin Xie

Keywords: carbon nanotube, chemical vapour deposition, diametre control, photonic crystal fibre, third-harmonic generation, mode-locked fibre laser

Abstract

Photonic crystal fibre (PCF) embedded with functional materials has demonstrated diverse applications ranging from ultrafast lasers, optical communication to chemical sensors.[1] Many efforts have been made to fabricating carbon nanotube (CNT) based optical fibres by ex-situ transfer method, however, often suffer poor uniformity and coverage[2]. Here, we report the direct growth of CNTs on the inner walls of PCFs by the chemical vapour deposition method. A two-step growth method was developed to control the narrow diametre distribution of CNTs to ensure desirable nanotube optical transitions. In the as-fabricated CNTs embedded fibre, third-harmonic generation has been enhanced by ~15 times compared with flat CNT film on fused silica. We further demonstrated a dual-wavelength all-fibre mode-locked ultrafast laser (~1561 nm and ~1064 nm) by integrating the 1.36±0.15 nm-diametre CNTs into two kinds of photonic bandgap PCF (HC-1550 and HC-1060) as saturable absorbers, using their S_{11} (~ 0.7 eV) and S_{22} (~ 1.2 eV) interband transition respectively. The fibre laser showed stable output of ~10 mW, ~800 fs pulse width and ~71 MHz repetition rate at 1561 nm wavelength. Our results can enable the large-scale applications of CNTs in PCF-based optical devices.

Results and discussion

Carbon nanotube (CNT) is a promising material in photonic and nonlinear optical applications due to its excellent properties of sub-picosecond recovery time, broadband response (0-2 eV), low saturation intensity (only one-twentieth of that of graphene), as well as perfect single-crystalline structure[3]. By embedding CNTs into an optical fibre, the light-CNT interaction length can be greatly enhanced through evanescent wave couplings, providing even more opportunities for their use. Additionally, the one-dimensional (1D) structure of CNTs, which forms an ultra-thin film, will not interfere with the transmission mode of optical fibres.

Previous efforts have focused on transferring CNTs onto side-polished[4], tapered normal optical fibres[5], or filling them into the holes of hollow capillary fibres (HCFs)[6]. However, the ultra-large aspect ratio of CNTs makes them prone to binding with each other. When CNT bundles are forced open with the assistance of surfactants and violent forces, the integrity of CNT structures may be compromised and introduce impurities that are hard to eliminate, hindering the reliable and large-scale transfer of high-quality CNTs. Additionally, treatments necessary to enable CNTs interact with light propagation in normal optical fibres has undesirable effects on the hybrid fibre. For example, side-polished fibre leads to unwanted polarization dependence[7], tapered fibre causes large insertion loss and alters the fundamental transmission mode[8], and hollow capillary fibre causes large coupling loss when connected to single-mode systems[6].

Currently, as the development of photonic-crystal fibres (PCFs)[9], whose porous structures provide spaces for material growth, two-dimensional materials such as graphene and MoS_2 have been successfully grown on the inner walls of the fibre. The centimetres-long graphene-PCF and MoS_2-PCF showed strong light-matter interactions and enhanced nonlinearity[1c, 1d, 10]. In contrast to graphene without a bandgap or MoS_2 with a certain large

bandgap, CNTs exhibit a broadband response (0-2 eV) and exquisite interband structures, benefiting broadband operation in optical and nonlinear optics[2b, 11]. However, growing CNTs is more challenging due to the need for extra diametre control, which greatly influences their bandgaps. For nonlinear optical applications involving CNTs embedded in optical waveguide, only the CNT segment resonating with the operating wavelength contributes positively, while the rest of CNTs induce detrimental effects such as extra absorption and scattering loss[2a]. Unfortunately, traditional CNT-based optical fibre fabrication methods rarely achieve diametre control of CNTs, and full coverage of CNT film is required for sufficient interaction area due to the weak evanescent light. Therefore, an efficient and undamaged fabrication strategy for producing high-coverage CNT optical fibre complexes with large-scale uniformity is crucial for real applications.

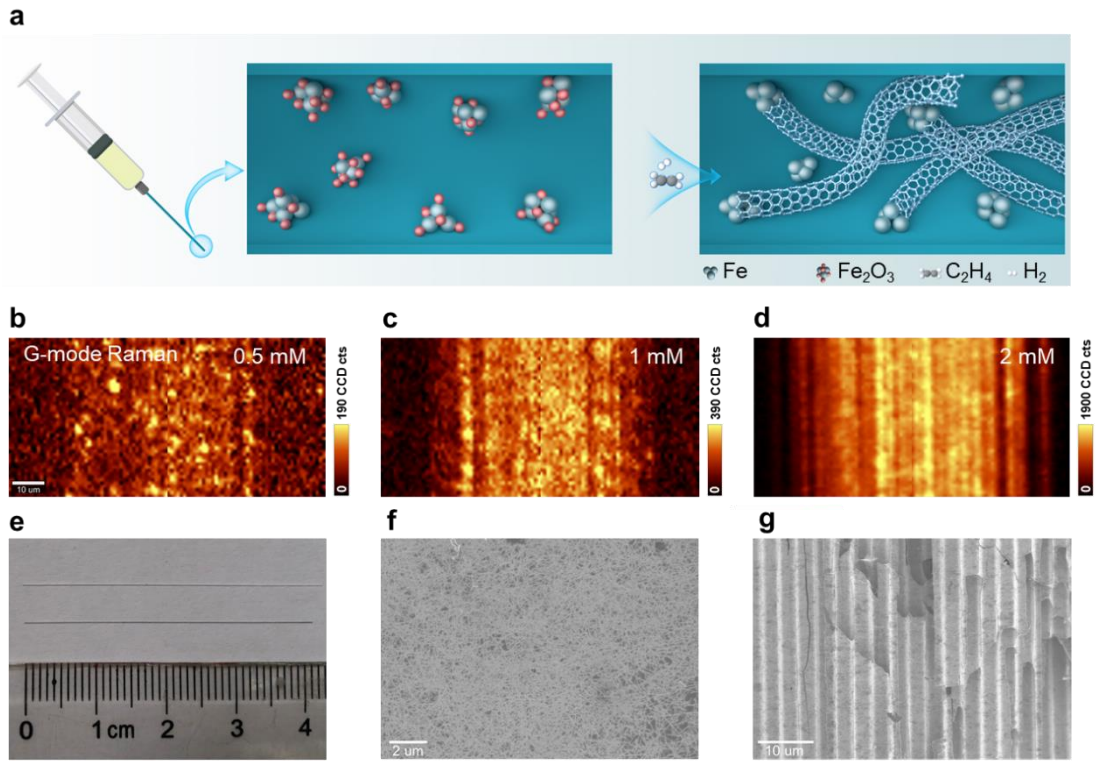

Figure 1. Growth of a high-density, uniform CNT-embedded optical fibre. a) Schematic of the growth method, consisting of the injection of $FeCl_3$ into fibre holes and drying at

moderate speed followed by high-temperature growth. b-d) G-mode Raman mapping of CNT-PCF, showing the dependence of CNT density on the $FeCl_3$ catalyst precursor concentrations of 0.5 mmol L^{-1} (a), 1 mmol L^{-1} (b) and 2 mmol L^{-1} (c), respectively. e) Optical image of bare PCF and CNT-PCF. f, g) Typical SEM image of the fractured CNT-PCF, showing full coverage, randomly oriented CNT "fabric" uniformly grown on the inner wall.

Here, we report the successful direct growth of full-coverage CNTs on the inner wall of a PCF using the chemical vapour deposition (CVD) method. This achievement builds on previous experiences in growing CNT horizontal arrays with controlled structures[12] and high density[13]. Our growth strategy consists of two steps, as illustrated in **Figure 1a**. Firstly, Fe catalyst precursors were filled into the fibre holes via injection of $FeCl_3$ ethanol solution (Figure 1a, left). Next, the fibre was moved into a CVD furnace and dried for 2 hours at a low temperature of 200 °C, where the Fe precursors were gradually oxidized and coated onto the inner fibre walls (Figure 1a, middle). The furnace temperature was then raised to ~820 °C, and 200 standards cubic centimetres per minute (sccm) of H_2 were introduced to reduce the catalyst precursors to Fe catalyst nanoparticles. Finally, after the introduction of a carbon source (ethylene, 50 sccm), the CNTs grew along the inner wall of the fibre (Figure 1a, right). The entire growth process was carried out under low-pressure conditions, where the gas flow was able to overcome the large viscous force within the micrometre-sized hole walls[1c], resulting in homogeneous CNT growth.

In our growth method, the CNT coverage can be easily adjusted by varying the concentration of the $FeCl_3$ solution. By increasing the solute concentration from 0.5 to 1 to 2 mmol L^{-1}, we observed a gradual increase in CNT coverage, from sporadic dispersion (Figure 1b) to moderate distribution (Figure 1c) to full coverage (Figure 1d), as reflected by G-mode Raman mappings of the CNT-PCFs. The increase in coverage was also confirmed by the increased contrast of the CNT-PCF photographs and more directly by the increased density of

CNTs in the scanning electron microscopy (SEM) images of the CNT-PCF fracture surface (Figure S1). A further increase in the $FeCl_3$ concentration resulted in poor quality of CNTs, as indicated by a high-intensity ratio of D- to G-mode in the Raman spectrum (Figure S2).

Under our optimised conditions, we successfully achieved homogeneous CNT growth on the hole walls of a 4-cm-long optical fibre (Figure 1e and Figure S3). We also broke the CNT-PCF to directly visualize the CNT dispersion (Figure S4c, d). The inner wall of the fibre exhibited long CNTs interlaced with each other, forming a perfect CNT film, like a "fabric" (Figure 1f), which was uniformly dispersed in all the hole walls (Figure 1g and Figure S4c, d). This randomly oriented CNT "fabric" on the inner wall of optical fibres brings additional advantages of polarization independence when used in photonics or nonlinear optics. We also conducted a controlled experiment, where we filled the fibres with catalyst precursor $FeCl_3$ through capillary filling instead of injection (as performed in MoS_2-PCF growth). We found that only a few CNTs sporadically distributed in the fibre, and the coverage of CNT could not be increased by changing the concentration of $FeCl_3$ solution or any other growth conditions using this strategy (Figure S5). Therefore, the injection of Fe catalyst precursors into the fibre holes is the crucial step for achieving full coverage growth of uniform CNT films onto the fibres.

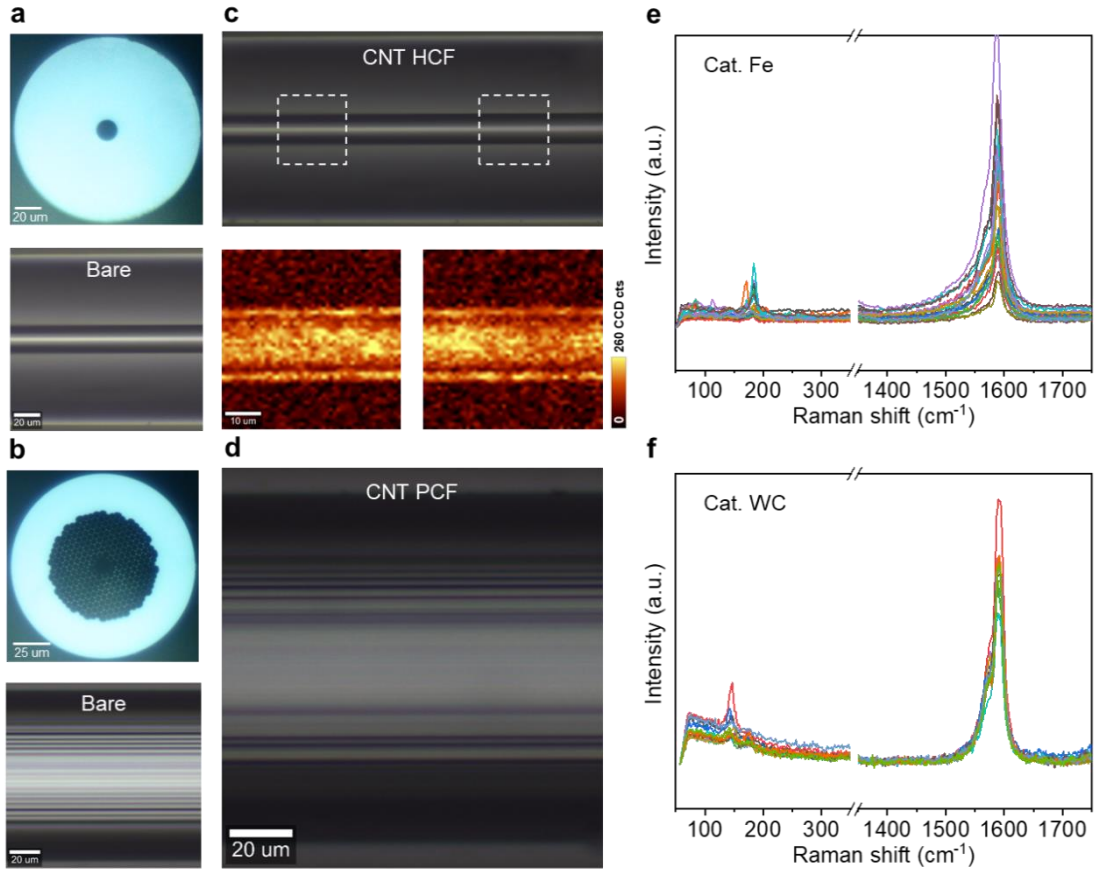

Figure 2. CNT-embedded optical fibres with diverse fibre structures and well-controlled diametres. a, b) Top (top) and side (bottom) views of an HCF with a core diametre of ~15 μm (a) and a PCF (HC-1550) with a hollow-core honeycomb structure (b). c, d) Side view of HCF and PCF after the growth of CNT, showing slightly higher contrast compared with the bare ones (a, b). The bottom of (c) is the G-mode Raman intensity mapping in white dash square, showing the full coverage of CNT in the inner wall. e, f) Raman spectra of the CNT-PCF grown by Fe and WC catalyst, using line mapping along the radial direction with scan step of 3 μm and an excitation laser of 633 nm, indicating well-controlled diametres.

Our growth method for the CNT-embedded optical fibre has been proven to be versatile, and applicable to different fibre structures and narrow diametre distributions. In addition to CNT-PCFs (**Figure 2b, d**), we have successfully achieved homogeneous CNT growth in HCFs with various hole diametres (ranging from 50 to 15 to 5 μm), as shown in Figure 2a, c and Figure S4a-d. As the diametre of the fibre hole decreases, gas flow in the narrower space

experiences greater viscous force[1c], requiring lower pressure and a higher carbon-hydrogen ratio for CNT growth.

Our growth method has also enabled the fabrication of CNT fibres with different diametre distributions by altering the types of catalyst precursor solutions. According to the CNT growth mechanism[12a], the size uniformity of the catalyst nanoparticles is a crucial factor for controlling the CNT diametre. For example, large Fe metal catalyst particles with high vapour pressure will rapidly vaporize under low-pressure and high-temperature conditions, leaving behind smaller nanoparticles. Under optimised growth conditions, we obtained CNTs with small diametres of 1.36±0.15 nm, as calculated from RBM peak positions in Raman line mapping (Figure 2e and Figure S6a)[14]. Notably, Raman line mapping measurements were taken along the radial direction with a scan step of 3 μm, as the small hole of PCF is ~3 μm, to avoid the possibility of testing the same CNT due to random orientations. The variation of Raman intensities is due to the mismatch of polarizations between the randomly oriented CNT film and the excitation laser, as well as the position fluctuation of the laser focus on the photonic crystal surface. However, the fluctuations do not influence the Raman shifts in the spectra. Conversely, using $(NH_4)_6W_7O_{24}$ as the catalyst precursor results in the formation of a WC catalyst, which catalyzes CNT growth under the same conditions[12a]. This leads to larger CNT diametres of 1.69±0.10 nm (Figure 2f and Figure S6b), as relatively large WC catalyst nanoparticles remain due to their high melting point and low vapour pressure. As a typical solid catalyst at growth temperature, the as-grown CNTs exhibit narrower diametre distributions than liquid catalyst Fe.

Direct measurement of the particle size of these catalysts is challenging due to the high curvature of the fibre's inner wall. Thus, we utilized a spatially confined CVD method to monitor the CNT growth conditions in an optical fibre. By using quartz-Si/SiO_2 stacking with a cubic weight on the quartz, a gap of <10 μm was formed[15], similar to PCF hole diametre,

allowing for gas flow monitoring (Figure S7). We maintained the temperature and pressure of the furnace identical to those used for CNT-PCF growth and determined the size of catalyst nanoparticles by AFM. The average diametre of Fe nanoparticles was ~2.0 nm (Figure S7b, d), smaller than that of tungsten-based nanoparticles (~2.4 nm, Figure S7c, e), consistent with our former analysis. The as-grown CNT-embedded optical fibres are well-suited for nonlinear optical applications.

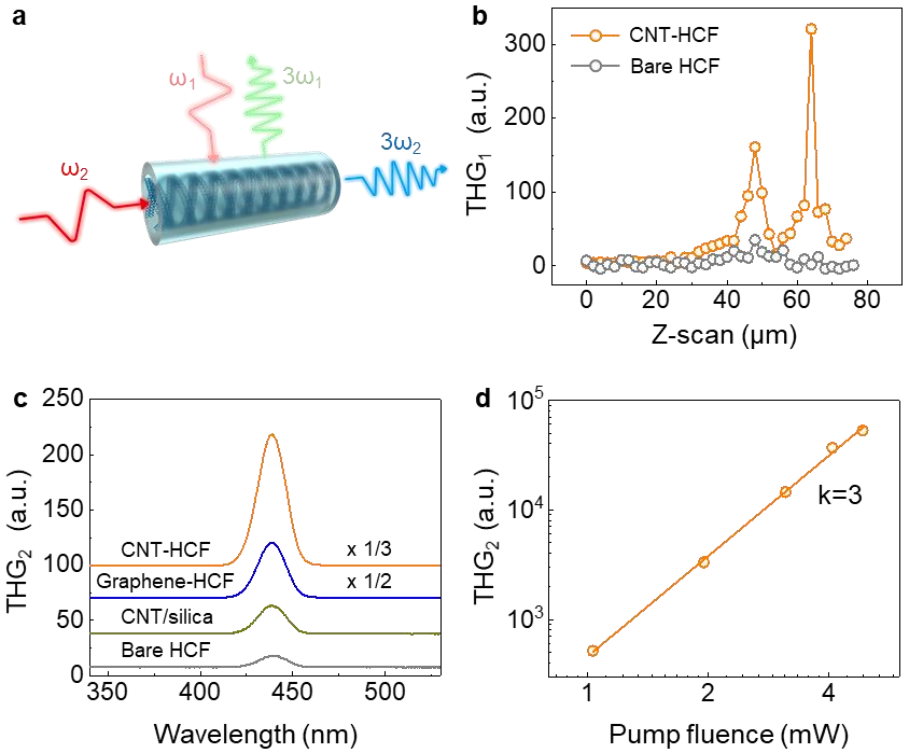

Figure 3. CNT-embedded optical fibres with harmonic enhancement. a) The schematic diagram of third-harmonic generation (THG) in CNT-HCF. b) The THG intensity varies with the depth of the incident laser ω_1 focused on the fibre sidewall. c) The THG spectra excited by the laser ω_2 along the fibre direction (CNT-HCF, graphene-HCF, CNT/silica and bare HCF) at the same incident power (~ 5 mW) and the same length (~ 3 cm). The peak intensity ratio of the four samples is about 33:9:2:1. d) Dependence of the THG signal intensity of the CNT-HCF on the incident optical power.

Conventional silica-based optical fibres have limited applications in nonlinear optics, such as frequency conversion, nonlinear harmonic generation, and supercontinuum generation, due to the small real part of the third-order nonlinear susceptibility (n_2~3×10^{-16} cm^2/W) of fused-silica materials. However, by embedding CNTs into the fused-silica optical fibre, the third-harmonic generation (THG) signal can be enhanced, as the evanescent wave interacts with the CNT film along the fibre direction (**Figure 3a**). The nonlinear polarization of π-electrons in the carbon honeycomb network gives CNTs ultra-high third-order nonlinearity (n_2~3×10^{-8} cm^2/W), which can be enhanced by excitons in the 1D structure.[16] Here, we used HCFs for CNT film growth and THG measurement due to their broader transmission window than photonic band gap PCFs (Figure S8), which allows both pump pulses and THG signals to propagate. To characterize the HCFs covered by CNT film, a femtosecond pulse (ω_1) is vertically incident to the side wall of the HCF to measure its THG intensity. Upon introducing CNTs into the HCF, two distinct peak THG intensities separated by 15 μm appear, corresponding to the HCF's internal diametre of 15 μm (Figure 3b). The transmittance of HCFs embedded with different CNT diametre distributions is also measured (Figure S8). The CNT-HCF with a tube diametre of ~1.36 nm exhibited low transmittance near 1500 nm, which corresponds to its S_{11} absorption peak.

THG enhancement performance of HCFs with different CNTs coverage and fibre length excited by the laser (ω_2) along the fibre direction were measured. Nevertheless, a trade-off exists between the harmonic enhancement effect and the linear absorption loss, as both the excitation light and the THG signal overlap with the CNT's absorption. The harmonic enhancement reached its maximum value in the full coverage sample with the fibre length of 3 cm, which displayed a ~30-fold increase of THG signals compared to that of bare HCF (Figure 3a and Figure S9). Such CNT-HCF exhibited a ~15 fold higher THG signal strength than the flat CNT film on fused silica (Figure 3c) and even higher than that of monolayer graphene-HCF (Graphene-HCF is grown using our previous approach[1c, 10a], detailed

characterization shown in Figure S10). The cubic relationship between the intensity of the THG signal and the incident optical power is consistent with theoretical expectations (Figure 3d). The THG signal can be further enhanced by several orders of magnitude if the phase matching between the THG and the fundamental frequency light is satisfied by extra fibre structure design[1d, 17].

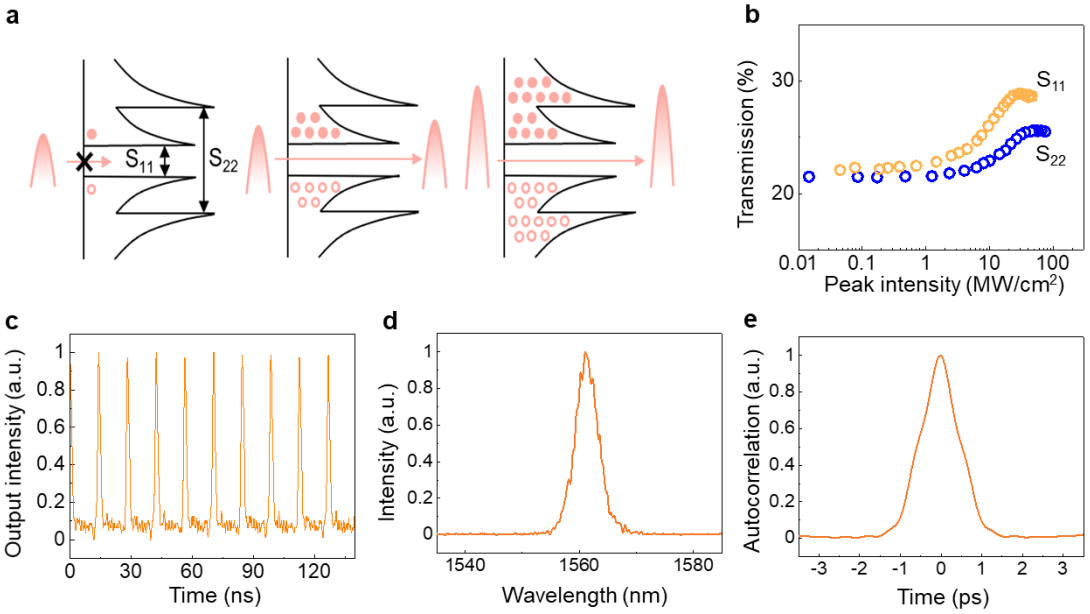

Figure 4. Stretched soliton generated by CNT-embedded HC-1550-based mode-locked ring fibre lasers. a) Schematic diagram of saturable absorption of CNTs corresponding to the S_{11} and S_{22} absorption edges respectively. b) Saturable absorption measurement of CNTs with a diametre of 1.36 nm embedded in fibres (blue for HC-1060 and orange for HC-1550), with modulation depths of 4.1% and 6.5%, respectively. c-e) Output results from a ring-cavity fibre laser with an average tube diametre of 1.36±0.15 nm CNTs embedded in HC-1550 fibre as a SA, where (c) is a pulse train with ~14 ns interval (~71 MHz), (d) is output spectrum with a central wavelength at 1561 nm and (e) is an autocorrelation trace with FWHM of ~800 fs.

The nonlinear absorption properties of CNTs are determined by the imaginary part of the refractive index, which endows them with saturable absorption properties for laser mode-locking[18]. Here, we prepared semiconductor CNTs with an average tube diametre of ~1.36

nm, which exhibited first and second interband transition energies (S_{11} and S_{22}) at approximately 0.7 eV and 1.2 eV, corresponding to two common near-infrared bands (~1550 nm and ~1060 nm, **Figure 4a**). To ensure mode-matching, two photonic band gap PCFs operating at 1550 nm and 1060 nm respectively (HC-1550 and HC-1060) are employed as substrates for the growth of CNTs, each with a length of 3 cm. The as-fabricated CNTs-HC-1550 and CNTs-HC-1060 samples were excited by femtosecond pulsed lasers at 1550 nm and 1064 nm, respectively. The corresponding modulation depths and saturation absorption intensities are 6.5%/4.1% and 7.6 MW/cm^2/14.4 MW/cm^2, respectively (Figure 4b). The saturation absorption intensity of S_{22} was approximately twice that of S_{11}, mainly due to the faster inter-subband transition in which the relaxation process from S_{22} to S_{11} dominates [19]. In general, most mode-locked fibre lasers opt for the S_{11} of the CNTs, corresponding to a single real gap in electron density of states, because S_{11} facilitates self-start mode-locking at low pump power. Whereas, the shorter lifetime of S_{22} may also have positive significance for mode-locking and enable the extension of the operating band to visible operating bands below 1μm[20].

The CNT film embedded HC-1550 and HC-1060 are employed as mode-locking elements for two ring-cavity fibre lasers using erbium-doped and ytterbium-doped fibre gain media, respectively, and operating at wavelengths of 1064 nm and 1561 nm. For the mode-locked Er-doped fibre laser, the total group velocity dispersion (GVD) is designed to be 0.001 ps^2 by dispersion management. The laser was pumped by a 980 nm laser diode and coupled into a ring cavity by a 980/1550 nm wavelength division multiplexer. A polarization controller (PC) and a polarization-independent isolator (PI-ISO) were employed to control the birefringence and the unidirectional pulse propagation within the cavity (Figure S11a). By carefully adjusting the PC, a 1.23 ps stretched pulse with a central wavelength of 1561 nm is generated at a pump power of 300 mW (Figure 4d and Figure S11b). The repetition frequency of the output laser is 71 MHz, corresponding to the total cavity length. The pulse

width could be further compressed to ~800 fs using out-of-cavity dispersion compensation based on the time-bandwidth limit theory, given the spectral width of 4.7 nm (Figure 4c and Figure 4e). The maximum average output power is about 10.0 mW, corresponding to the single pulse energy of about ~140 pJ. Typically, ultrafast fibre lasers that use nonlinear low-dimensional materials embedded into the air holes of PCF as saturation absorbers exhibit ease of integration and superior damage threshold power compared to the film directly attached to the fibre end face. For instance, all fibre lasers based on MoS_2-PCF produce a pulse width of ~500 fs operating at 1550 nm, while graphene-PCF produces a pulse width of ~2 ps [1d, 10a]. In our design, by adjusting the diametre of CNTs and selecting the PCF of a specific working wavelength, we can flexibly tune the laser's operating wavelength and generate sub-1 ps laser pulses, highlighting the superiority of our CNT-PCFs.

We also designed a fibre ring cavity operating at 1064 nm, consisting of a 0.65 m highly ytterbium-doped fibre (YDF, LIEKKI Yb1200-4/125) and a 2.85 m single-mode fibre (HI 1064) (Figure S12a). The net cavity dispersion is normal, with an estimated value of 0.0782 ps^2. The intracavity mode-locking component consisted of the same diametre CNTs used in the 1561 nm fibre laser described above. However, the operating wavelength of the laser, in this case, corresponds roughly to the S_{22} absorption edge, and the CNTs are embedded in HC-1060 at an operating band of around 1060 nm. Since the S_{22} utilized here requires larger pump energy to reach saturation, we obtain the bound soliton state at the fundamental repetition rate at the pump power of 520 mW. The spectral centre of the output pulse is 1064 nm, with typical steep edge characteristics, indicating that it is an all-normal dispersion dissipative soliton (Figure S12b). The 58.8 MHz fundamental mode-locked pulse trains were demonstrated in Figure S12c, corresponding to the total cavity length. The width of the autocorrelation trace was ~45 ps and the periodic modulated trace is one of the typical characteristics of bound soliton (Figure S12d). The maximum average output power is about 11.3 mW, corresponding to the single pulse energy of about ~192 pJ, which is limited by the

output power of the pump laser diode. Commercially available dispersion-compensating fibres in the 1060 nm band are scarce, so most fibre lasers in this band operate as dissipative solitons in the full positive dispersion band, resulting in output pulse widths in the region of one hundred picoseconds[21], except for the regulation of intracavity dispersion through the introduction of space grating pairs in the fibre ring cavity[22].

Conclusion

We successfully demonstrated a two-step method for growing CNTs directly onto optical fibres to fabricate a new functional fibre, i.e. CNT-PCF. The homogenous and high-quality CNTs with narrow diametre distributions on the inner hole walls of the PCF were obtained by adjusting the concentration and types of catalyst precursors in the low-pressure CVD method. The CNT-PCF exhibited nonlinear optical application potentials in both third-harmonic generation and ultrafast fibre lasers, taking advantage of the superior nonlinear susceptibility of CNT in both real and imaginary parts. Specifically, THG could be enhanced by ~15 times compared with flat samples, even surpassing that of graphene fibres. Ultrafast dual-wavelength all-fibre laser was also demonstrated with ~800 fs pulse width and ~71 MHz repetition rate. Further, by using CNT-PCF with different CNT diametres, ultrafast fibre lasers covering all the major wavelengths between 1 μm and 2 μm or even below 1 μm could be realized. Our results can enable the large-scale applications of CNTs based on this new functional fibre.

Methods

Injection of catalyst precursors into optical fibres. Catalyst precursors (Fe or W) were injected into the fibres of their corresponding saline ethanol solutions at optimised concentrations. To ensure full coverage of CNT growth, the amount of catalyst precursor was adjusted based on the catalytic activity of the corresponding catalyst. Typical concentrations are as follows: $FeCl_3$ at ~2 mmol L^{-1}, $(NH_4)_6W_7O_{24}$ at ~2.5 mmol L^{-1}. Then, the as-injected fibres were immediately heated to 200 °C and dried in the air for 2 hours before CNT growth.

Syntheses of CNT-embedded optical fibres. The fibres coated with catalyst precursors on the inner wall were transferred into a one-inch quartz tube and placed at the centre of a CVD furnace. The furnace chamber was then raised to the optimised growth temperature of ~820 °C in air and flushed with argon (300 sccm) to create an inert atmosphere. Subsequently, hydrogen was introduced to facilitate the transformation of the catalyst precursors into catalyst nanoparticles. Finally, the carbon sources (ethylene 50 sccm) were introduced, and the entire process was carried out at a pressure of ~400 Pa for a growth duration of 15-30 min. After the CNT growth, the system was naturally cooled down to room temperature.

Characterization of CNT-embedded optical fibres. Optical photographs were taken using a microscope by focusing on the holes in the fibre. Raman mapping was collected using both the WITec alpha300 system and Jovin Yvon-Horiba LabRam systems, with excitation wavelengths of 488 nm, 514 nm and 633 nm. SEM images were obtained on a Hitachi S4800 SEM, operated at 1.0 kV.

Harmonic generation measurements. The THG of hollow core fibre embedded with CNT film was excited with femtosecond pulses (Coherent laser, ~150 fs, 250 kHz) generated by a Ti: sapphire oscillator pumping an OPA. An objective (Nikon objective, ×4, NA=0.1) was used to focus the excited light onto the CNT-HCF. The generated THG signal was collected by a Princeton SP2500 spectrometre after being filtered by a 650 nm short-pass filter.

Saturable absorption measurements. Femtosecond pulses (Coherent Mira-OPO-X, 1064 nm, ~150 fs, 76 MHz) generated by a Ti: sapphire oscillator (Coherent, Mira-HP) were coupled to a 90:10 coupler for measuring the saturable absorption characteristics of CNT-HC-1060. A fibre laser (Origami, ~150 fs, ~100MHz) generates ultrafast light centred at 1550 nm connected via a flange to a 90:10 coupler, of which 10% is used for real-time power monitoring and the remaining 90% for measuring the saturable absorption characteristics of the CNT-HC-1550.

Characterization of all-fibre mode-locked laser at dual wavelengths. For the 1561 nm fibre laser, a 980 nm diode laser with a maximum output power of 600 mW was coupled into the ring cavity of the fibre laser via a wavelength division multiplexer (980 nm/1550 nm) and then pumps the erbium-doped gain fibre (60 cm, Er110 4-125, LIEKKI). The near-zero total group velocity dispersion (0.001 ps^2) of the 1550 nm ring cavity was designed for dispersion management soliton generation. The isolator in the ring cavity is designed to prevent backwards transmitted light in the cavity from adversely affecting the fibre laser system. The CNT-PCF (3 cm, NKT, HC-1550) was integrated into the ring cavity by a homemade two-axis alignment system. The polarization controller optimises spectral and pulse width results by fine-tuning intracavity dispersion and nonlinearity. For the 1064 nm fibre laser, the pump source follows the 980 nm diode laser, the operating band of the wavelength division

multiplexer was changed to 980 nm/1064 nm, the gain medium was chosen to be a ytterbium-doped fibre (~65 cm, YDF, LIEKKI Yb1200-4/125), the operating band of both the ISO and the output coupler was chosen to be 1064 nm and all devices were connected via SMF (HI-1064, Corning). The normal net cavity dispersion (0.0782 ps^2) of the ring cavity was designed for dissipative solitons generation. The ring cavity is not equipped with filter pieces and there is a certain filtering effect with the combination of PCF, isolator and polarization controller. The spectra were measured by a Fourier transform infrared spectrometre (OSA205C, Thorlabs), the pulse width by autocorrelation (Pulsecheck USB 50, APE) and the repetition frequency by an oscilloscope (DS6104, Rigol) and photodetector (DET08CFC/M, Thorlabs).

Data availability

The data supporting the findings of this study are available within the paper and Supporting Information. Extra data are available from the corresponding authors upon reasonable request.

Acknowledgements

This work was financially supported by the Ministry of Science and Technology of China (2016YFA0200100 and 2018YFA0703502), the National Natural Science Foundation of China (Grant Nos. 52021006, T2188101, 52025023, 51720105003, 21790052, 21974004, 52102032, 92256202, U22A20399, 22221001, 22073038), the Strategic Priority Research Program of CAS (XDB36030100), the Beijing National Laboratory for Molecular Sciences (BNLMS-CXTD-202001), the 111 project 2.0 (BP1221004), and the Fundamental Research Funds for the Central Universities (lzujbky-2022-kb0).

Author contributions

J.Z. and K.H.L. conceived the experiments and supervised the project. Q.X. conceived the growth experiments. J.X. and K.F.L performed the optical experiments and fibre laser setup. Q.X. conducted the SEM, AFM and Raman characterizations. L.Q., G.J.Y and H.L.Z. suggested the characterizations and analysis. All the authors discussed the results and wrote the manuscript.

Conflict of Interest

The authors declare no conflict of interest.

References

[1] a) C. Markos, J. C. Travers, A. Abdolvand, B. J. Eggleton, O. Bang, Rev. Mod. Phys. 2017, 89, 045003; b) D. Cotter, R. J. Manning, K. J. Blow, A. D. Ellis, A. E. Kelly, D. Nesset, I. D. Phillips, A. J. Poustie, D. C. Rogers, Science 1999, 286, 1523; c) K. Chen, X. Zhou, X. Cheng, R. Qiao, Y. Cheng, C. Liu, Y. Xie, W. Yu, F. Yao, Z. Sun, F. Wang, K. Liu, Z. Liu, Nat. Photonics 2019, 13, 754; d) Y. Zuo, W. Yu, C. Liu, X. Cheng, R. Qiao, J. Liang, X. Zhou, J. Wang, M. Wu, Y. Zhao, P. Gao, S. Wu, Z. Sun, K. Liu, X. Bai, Z. Liu, Nat. Nanotechnol. 2020, 15, 987.

[2] a) A. Martinez, Z. Sun, Nat. Photonics 2013, 7, 842; b) S. Yamashita, J. Lightwave Technol. 2012, 30, 427; c) Y. Tan, Chemosensors 2018, 6, 55.

[3] a) S. Yamashita, A. Martinez, B. Xu, Opt. Fiber Technol. 2014, 20, 702; b) L. Qian, Y. Xie, S. Zhang, J. Zhang, Matter 2020, 3, 664; c) V. S. Abhisha, R. Stephen, in Handbook of Carbon Nanotubes, (Eds: J. Abraham, S. Thomas, N. Kalarikkal), Springer International Publishing, Cham 2022, 131.

[4] a) K. F. Mak, J. C. Travers, P. Holzer, N. Y. Joly, P. S. Russell, Opt Express 2013, 21, 10942; b) Y.-W. Song, S. Yamashita, C. S. Goh, S. Y. Set, Opt. Lett. 2006, 32, 148.

[5] a) Y.-W. Song, K. Morimune, S. Y. Set, S. Yamashita, Appl. Phys. Lett. 2007, 90, 021101; b) K. Kieu, M. Mansuripur, Opt. Lett. 2007, 32, 2242; c) K. Kashiwagi, S. Yamashita, Opt. Express 2009, 17, 18364.

[6] S. Y. Choi, F. Rotermund, H. Jung, K. Oh, D.-I. Yeom, Opt. Express 2009, 17, 21788.

[7] K. T. Kim, D. S. Yoon, G.-i. Kwoen, Opt. Commun. 2004, 230, 137.

[8] A. J. Fielding, K. Edinger, C. C. Davis, J. Lightwave Technol. 1999, 17, 1649.

[9] a) P. Russell, Science 2003, 299, 358; b) J. C. Knight, Nature 2003, 424, 847.

[10] a) Y. Cheng, W. Yu, J. Xie, R. Wang, G. Cui, X. Cheng, M. Li, K. Wang, J. Li, Z. Sun, K. Chen, K. Liu, Z. Liu, ACS Photonics 2022, 9, 961; b) G. Q. Ngo, A. George, R. T. K. Schock, A. Tuniz, E. Najafidehaghani, Z. Gan, N. C. Geib, T. Bucher, H. Knopf, S. Saravi, C. Neumann, T. Luhder, E. P. Schartner, S. C. Warren-Smith, H. Ebendorff-Heidepriem, T. Pertsch, M. A. Schmidt, A. Turchanin, F. Eilenberger, Adv. Mater. 2020, 32, 2003826.

[11] a) X. Li, H. Zhu, J. Materiomics 2015, 1, 33; b) A. K. Geim, Science 2009, 324, 1530.

[12] a) S. Zhang, L. Kang, X. Wang, L. Tong, L. Yang, Z. Wang, K. Qi, S. Deng, Q. Li, X. Bai, F. Ding, J. Zhang, Nature 2017, 543, 234; b) S. Zhang, X. Wang, F. Yao, M. He, D. Lin, H. Ma, Y. Sun, Q. Zhao, K. Liu, F. Ding, J. Zhang, Chem 2019, 5, 1182.

[13] a) Y. Xie, L. Qian, D. Lin, Y. Yu, S. Wang, J. Zhang, Angew. Chem., Int. Ed. 2021, 60, 9330; b) Y. Hu, L. Kang, Q. Zhao, H. Zhong, S. Zhang, L. Yang, Z. Wang, J. Lin, Q. Li, Z. Zhang, L. Peng, Z. Liu, J. Zhang, Nat. Commun. 2015, 6, 6099.

[14] a) Q. Zhao, J. Zhang, Small 2014, 10, 4586; b) A. Jorio, R. Saito, J. H. Hafner, C. M. Lieber, M. Hunter, T. McClure, G. Dresselhaus, M. S. Dresselhaus, Phys. Rev. Lett. 2001, 86, 1118; c) Y. Yao, Q. Li, J. Zhang, R. Liu, L. Jiao, Y. T. Zhu, Z. Liu, Nat. Mater. 2007, 6, 283.

[15] L. Qian, Q. Shao, Y. Yu, W. Liu, S. Wang, E. Gao, J. Zhang, Advanced Functional Materials 2021, 32, 2106643.

[16] V. A. Margulis, T. A. Sizikova, Physica B 1998, 245, 173.

[17] B. Jiang, Z. Hao, Y. Ji, Y. Hou, R. Yi, D. Mao, X. Gan, J. Zhao, Light: Sci. Appl. 2020, 9, 63.

[18] a) P. Avouris, M. Freitag, V. Perebeinos, Nat. Photonics 2008, 2, 341; b) K. Y. Lau, X. Liu, J. Qiu, Adv. Photonics Res. 2022, 3, 2200023.

[19] S. Xu, F. Q. Wang, C. H. Zhu, Y. F. Meng, Y. J. Liu, W. Q. Liu, J. Y. Tang, K. H. Liu, G. H. Hu, R. C. T. Howe, T. Hasan, R. Zhang, Y. Shi, Y. B. Xu, Nanoscale 2016, 8, 9304.

[20] a) J. S. Lauret, C. Voisin, G. Cassabois, C. Delalande, P. Roussignol, O. Jost, L. Capes, Phys. Rev. Lett. 2003, 90, 057404; b) C. Manzoni, A. Gambetta, E. Menna, M. Meneghetti, G. Lanzani, G. Cerullo, Phys. Rev. Lett. 2005, 94, 207401.

[21] Y. Z. Pan, J. G. Miao, W. J. Liu, X. J. Huang, Y. B. Wang, Laser Phys. Lett. 2014, 11, 095105.

[22] L. Hou, H. Guo, Y. Wang, J. Sun, Q. Lin, Y. Bai, J. Bai, Opt. Express 2018, 26, 9063.

Table of Contents

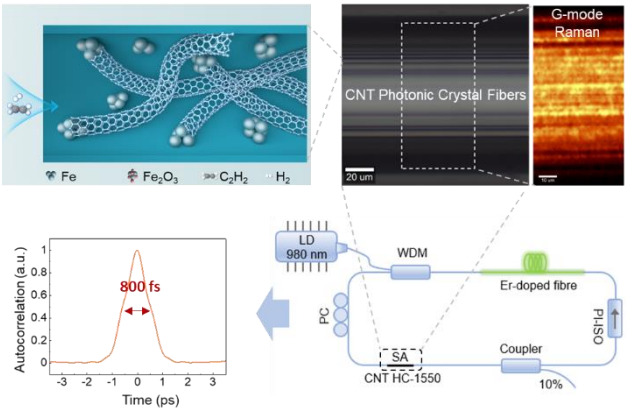

Direct growth of carbon nanotubes (CNTs) with narrow diametre distribution on the inner walls of photonic crystal fibres by a two-step chemical vapour deposition method was developed. By using the as-fabricated 3-cm-long CNT-fibres with desirable nanotube optical transitions, both third-harmonic generation has been largely enhanced and mode-locked ultrafast laser has been fabricated with a stable output of ~10 mW, ~800 fs pulse width and ~71 MHz repetition rate.